Distribution Agreement

In presenting this thesis as a partial fulfillment of the requirements for a degree from Emory University, I hereby grant to Emory University and its agents the non-exclusive license to archive, make accessible, and display my thesis in whole or in part in all forms of media, now or hereafter now, including display on the World Wide Web. I understand that I may select some access restrictions as part of the online submission of this thesis. I retain all ownership rights to the copyright of the thesis. I also retain the right to use in future works (such as articles or books) all or part of this thesis.

Rebecca Butterfield April 14, 2014

Investigating Electrical Activity Accompanying Functional Recovery of the Pyloric Circuit Following Isolation from Neuromodulatory Inputs

by

Rebecca Butterfield

Astrid Prinz, PhD
Adviser

Neuroscience and Behavioral Biology

Astrid Prinz, PhD

Adviser

Ronald Calabrese, PhD

Committee Member

Joseph Manns, PhD

Committee Member

Peter Wenner, PhD

Committee Member

2014

Investigating Electrical Activity Accompanying Functional Recovery of the Pyloric Circuit Following Isolation from Neuromodulatory Inputs

By

Rebecca Butterfield

Astrid Prinz, PhD

Adviser

An abstract of
a thesis submitted to the Faculty of Emory College of Arts and Sciences
of Emory University in partial fulfillment
of the requirements of the degree of
Bachelor of Sciences with Honors

Neuroscience and Behavioral Biology

2014

Abstract

Investigating Electrical Activity Accompanying Functional Recovery of the Pyloric Circuit Following Isolation from Neuromodulatory Inputs

By Rebecca Butterfield

We use a simple, invertebrate neural circuit to study neural systems' adaptive ability. The pyloric circuit of the stomatogastric ganglion is an example of a central pattern generator that controls muscles needed for food particle sorting in crustaceans. As a central pattern generator, the pyloric circuit controls an oscillatory behavior that must be maintained in the face of a changing environment. A well-studied property of this circuit is its ability to regain a stable activity rhythm after losing it for several days due to isolation from neuromodulatory inputs via decentralization. Previous research supports that this functional rhythm recovery results from readjustment of cells' conductance parameters as both a direct response to loss of neuromodulatory inputs and an indirect response to changes in cells' own electrical activity. We investigated the circuit's electrical activity patterns following decentralization in order to gain a better understanding of the recovery process. We used continuous extracellular recordings of pyloric activity following decentralization in both untreated preparations and preparations treated with chondroitinase ABC, an enzyme known to delay or prevent reemergence of stable rhythm. We looked for differences in activity following decentralization between treatment groups and for aspects of post-decentralization activity that are predictive of the stable rhythm that is later regained. Across many measures used to quantify features of electrical activity, we did not find strong evidence that electrical activity following decentralization is predictive of adaptive ability.

Investigating Electrical Activity Accompanying Functional Recovery of the Pyloric Circuit Following Isolation from Neuromodulatory Inputs

By

Rebecca Butterfield

Astrid Prinz, PhD

Adviser

A thesis submitted to the Faculty of Emory College of Arts and Sciences
of Emory University in partial fulfillment
of the requirements of the degree of
Bachelor of Sciences with Honors

Neuroscience and Behavioral Biology

2014

Acknowledgements

Getting involved in research as an undergraduate has been one of my most rewarding and educational experiences. I'm extremely lucky to have been part of the Computational Neuroscience Training Grant at Emory and Georgia Tech. My research has benefited tremendously from the resources and community offered by this program. I've learned a great deal from the CNTG faculty and fellow students. In particular, thank you to Dr. Ilya Nemenman for your encouragement to apply to the program and for your excellent mentorship during my first lab rotation.

Astrid Prinz, thank your guidance and support during my time in your lab. I consider myself very fortunate to have had you as my advisor. I've gained an appreciation for science and research during my time in the Prinz lab that I couldn't have gotten from any class. Amber Willett, thank you for being a great mentor. This research project would not have been possible without your data and guidance. Thank you also to Wafa Soofi for always being a friendly presence in the lab and for answering my random science-related questions. Ryan Hooper and Cengiz Gunay, you have helped me countless times with technical questions and computer issues. I really appreciate your time.

Thank you to Dr. Dirk Bucher for your suggestion to use spectrogram and autocorrelation analyses. Though a quick suggestion, it shaped a huge part of my research. Dr. Sam Sober, thank you for helping me as I was working out the kinks with my spectrogram analysis. To Dr. Ron Calabrese, Dr. Joe Manns, and Dr. Peter Wenner, thank you for contributing your time to this project by serving on my committee. Your fresh perspective upon hearing about my work has been invaluable.

Finally, to my parents, thank you for teaching me the value of curiosity, learning, and hard work. Thank you for your support and encouragement since day one to achieve my goals.

Table of Contents

List of Figures

List of Tables

INTRODUCTION

How neural circuits are able to maintain appropriate activity despite environmental changes is an important question in neuroscience. A biological system able to adapt to neuronal damage would thus be an interesting model in which to investigate successful adaptive ability. The pyloric circuit of the stomatogastric ganglion (STG) has proven to be such a system, able to resume its typical neuronal activity patterns after isolation from neuromodulatory inputs. The pyloric circuit is a central pattern generator (CPG) that controls the rhythmic dilation and constriction of muscles in the pyloric section of the stomach of decapod crustaceans. As a CPG, the pyloric circuit must remain appropriately active throughout the animal's lifespan. In general, CPGs control behaviors that must remain stably active long-term, such as a heartbeat or breathing. A better understanding of how the pyloric circuit is able to regain its typical rhythmic activity following an environmental perturbation could inform about how long-term stability is possible in more complex mammalian CPGs and oscillatory systems.

Anatomy of the pyloric circuit

Electrical behavior of pyloric cells has been well characterized and synaptic connections comprising the circuit have been fully diagrammed, thus making the circuit ideal for research. The anatomy of the stomatogastric nervous system (STNS), which contains the STG, and a simplified schematic of the pyloric circuit are shown in figure 1A and 1B. The circuit consists of four cell types: the anterior burster interneuron (AB), pyloric dilator motoneuron (PD), lateral pyloric motoneuron (LP), and pyloric motoneuron (PY) neurons. The AB and PD neurons are electrically coupled and serve as the pacemaker for the network (Harris-Warrick et al., 1992). The PD, LP, and PY motoneurons innervate their target muscles via the lateral ventricular nerve (*lvn*) and pyloric dilator nerve (*pdn*) (Selverston et al., 1976). The STG receives

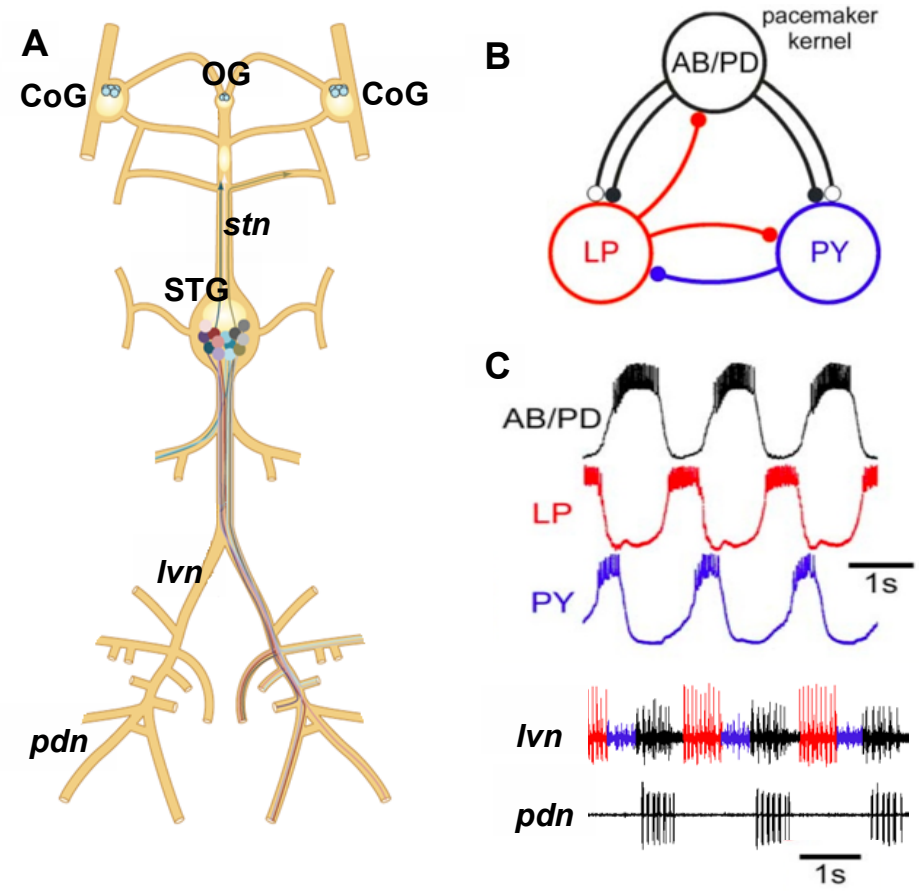

Figure 1: The stomatogastric nervous system and pyloric circuit. (A) Diagram of the stomatogastric nervous system. Neuromodulatory inputs from paired CoGs and the OG feed into the STG through the *stn* nerve. The *lvn* nerve contains axonal projections from PD, LP, and PY cells and the *pdn* nerve from PD cells. Adapted from (Hudson et al., 2010). (B) A schematic of the pyloric circuit. Filled circles represent glutamatergic inhibitory synapses, open circles represent cholinergic inhibitory synapses. (C) Intracellular (top) and extracellular (bottom) recordings showing triphasic bursting rhythm of the pyloric circuit. Panels B and C (top) adapted with permission from Macmillan Publishers Ltd: Nature Neuroscience (Prinz et al., 2004).

neuromodulatory inputs via the stomatogastric nerve (*stn*) from the paired commissural ganglia (CoGs) and esophageal ganglion (OG) located in the central nervous system (Harris-Warrick et al., 1992).

Pyloric circuit activity and functional recovery following decentralization

When the STNS is intact *in vitro*, pyloric cells burst in a triphasic pattern with a period of 1-2 seconds (figure 1C&D). PD neurons initially fire a burst of action potentials, then the LP neuron, and finally the PY neurons. This *in vitro* pattern of activity closely resembles activity seen *in vivo* (Rezer and Moulins, 1983). When neuromodulator inputs from the CoGs and OG to the STG are removed by cutting of the *stn* (known as decentralization), the pyloric bursting rhythm slows or ceases, losing its coordinated periodicity between the PD, LP, and PY cells. Because of this dependence on neuromodulatory inputs for a rhythmic activity pattern, the pyloric circuit has been described as a conditional oscillator (Moulins and Cournil, 1982; Bal et al., 1988). However, long-term maintenance of the STNS in culture following decentralization has revealed that a slower yet pyloric-like rhythm usually resumes after 3-5 days (Thoby-Brisson and Simmers, 1998). This recovery of function represents a transition of pyloric cells from chemo-dependent oscillators to endogenous oscillators (Thoby-Brisson and Simmers, 2000).

Evidence supports that shifts in pyloric cells' intrinsic membrane conductances and synaptic strengths rather than a reorganization of pyloric circuitry underlie the recovery process (Thoby-Brisson and Simmers, 2000; Thoby-Brisson and Simmers 2002). These changes in intrinsic membrane properties could be either an indirect response to changes in electrical activity (Golowasch et al., 1999; Zhang and Golowasch 2007; Liu et al., 1998) or a direct response to loss of neuromodulatory input (Thoby-Brisson and Simmers, 1998). More recent work, however, suggests that activity-dependent and neuromodulator-dependent mechanisms

both play a role in the pyloric circuit's ability to functionally recover following decentralization (Zhang et al., 2009; Zhang and Golowasch 2011). Long-term maintenance of conductance correlations has been linked with neuromodulatory regulation independent of activity feedback mechanisms, with many conductance pairs losing coordination following decentralization (Khorkova and Golowasch 2007; Temporal et al., 2012). It has also been shown that the extracellular matrix likely plays a role in pyloric recovery following decentralization (potentially through an activity-dependent mechanism), but not in generation of ongoing pyloric rhythm. When chondroitin sulfate, a primary component of perineuronal net extracellular matrix, is degraded by chondroitinase ABC (chABC), recovery is significantly delayed or prevented (Hudson 2013). Altogether, these findings indicate that a complex set of activity-dependent and neuromodulator-dependent changes in membrane properties and extracellular structure play a role in recovery.

Relationship between conductances and electrical output

While a neuron's particular set of membrane conductances form the basis of that neuron's electrical activity, the relationship between ionic conductances and electrical activity is nontrivial. Electrical output of a single cell or neuronal network may be tightly constrained in order to maintain proper function, but the cell or network's set of underlying conductances may vary greatly (Prinz et al. 2004; Schulz et al, 2006). The set of possible conductances that a cell can have is often described in terms of a multi-dimensional parameter space, in which specific subregions correspond to a given class of electrical activity (Foster et al., 1993; Goldman et al., 2001; Golowasch et al., 2002; Prinz et al. 2003). Since alteration of cell's conductance parameters is thought to underlie the pyloric circuit's recovery process, knowledge of how cellular conductances shift within parameter space would inform about how recovery is

achieved. It is impossible to measure a cell's complete set of ionic conductances continuously long-term, but we can continuously record electrical activity (Luther et al. 2003, Hudson 2013). Electrical activity type both arises from conductance parameters and acts as a feed-back mechanism that can further regulate cellular conductances – thus a better understanding of pyloric activity in response to decentralization could provide information about the recovery process. However, due to the intricate relationship between conductance and electrical activity and additional factors such as neuromodulators that also play a role in regulating conductances, we can only speculate on what observations about electrical activity mean in terms of conductances.

Investigating electrical activity following decentralization

While there are qualitative similarities in the activity patterns of different individuals in response to decentralization – loss or slowing of pyloric rhythm following decentralization and eventual reemergence of pyloric rhythm several days later – much variability exists between different individual's recovery processes. Data collected for the Hudson 2013 study on the role of extracellular matrix in facilitating recovery has shown a large amount of variability among individual post-decentralization activity patterns. For example, some individuals remain continuously active following decentralization (albeit at a slower frequency), while others fall silent and remain inactive for hours or days. When and to what extent an individual achieves recovery is also highly variable. We believe that exploring the post-decentralization electrical activity across individuals could potentially inform about the underlying recovery process. Previous work has found that across individuals, many short spurts of high-frequency pyloric activity precede a stable rhythm recovery. It has been speculated that these short periods of rhythmic activity, called bouts, play a role in regulating pyloric activity following

decentralization, thus allowing for recovery (Luther et al., 2003). While bouting has been observed as an accompaniment of the recovery process, nothing about an individual's specific bouting behavior has been found to be related to recovery time or recovery frequency (Luther et al., 2003; Hudson 2013). However, the activity bouts previously examined last only for seconds or minutes. A detailed exploration of individuals' post-decentralization activity patterns aside from these bouts has not been done.

We aimed to look for any aspect of electrical activity following decentralization which is somehow predictive of the stable rhythm that is (usually) eventually achieved. For our analysis we used data collected in the Hudson 2013 study. These data include stomatogastric nervous systems (STNSs) *in vitro* that were treated with chABC in order to degrade extracellular perineuronal nets as well as controls that were treated with denatured chABC (DNchABC) or received no treatment. Rather than describing individual STNSs as "recovered", we quantitatively defined stable epochs. While the term "recovery" implies the reemergence of a stable pyloric rhythm that continually persists, we often observed that an individual would enter a time range of stability lasting several hours, possibly losing stability thereafter. These stable epochs can occur multiple times, separated by hours of inactivity or unstable activity. Instead of defining a single time after which an individual is considered "recovered", we defined time ranges which meet our definition of a stable rhythm (stable epochs) and analyzed the relationship between electrical activity during the time leading up to these stable epochs and the stable epochs themselves. We looked for activity patterns that are predictive of when and to what extent stability is achieved. Because chABC treatment is known to delay or prevent onset of stable rhythm following decentralization, we also looked for features of activity which differed between treatment groups. Although findings from our analysis cannot directly reveal underlying

biological mechanisms, electrical activity nevertheless has the potential to provide further information about the circuit's ability to adapt to loss of neuromodulatory inputs.

A large part of our research has focused on developing techniques to quantify different features of pyloric activity. We wished to define metrics for rhythm speed, activity level, and rhythm regularity. Quantifying rhythm regularity was of particular interest because highly organized pyloric rhythm is lost following decentralization. Prior to quantifying activity level or regularity, we first needed a way to describe the circuit's bursting behavior over time, for example using a list of detected burst times. Our data consist of many continuous, multi-day extracellular nerve recordings. While we were able to perform spike and burst detection on several recordings, others proved difficult to analyze in this way. Thus we have used spectrograms and autocorrelograms, which can be generated for any of our continuous recordings, in order to expand our data set. Each analysis technique offers a distinct visualization of long-term pyloric activity. Additionally, for each technique we developed a unique set of metrics with which to characterize changes in pyloric activity over time.

METHODS

Animals and electrophysiology

Electrophysiological data used in the present study were collected previously by Amber Hudson (Hudson 2013). Long-term extracellular recordings were taken in vitro from the *lvn* and *pdn* nerves of the intact STNS of *Cancer borealis*. The STG was treated with chABC in media, DNchABC in media (control), or media alone (control). Preparations were then left undisturbed for 12-18 hours, after which enzyme was removed. At this point, the STG was decentralized by

cutting the *stn*. Extracellular recordings ran continuously for at least 5 days following decentralization. Media supplemented with glucose, penicillin, and streptomycin was replaced every 12-18 hours. In several experiments the *stn* was left intact as a control to measure the effect of enzymatic treatment on ongoing pyloric rhythm. Further details of the organ culture and electrophysiological set up have been described previously (Hudson 2013). The present study includes 19 decentralized preparations, including chABC treated (n = 8), DNchABC treated (n = 6), and media-only preparations (n = 5).

Analyzing long-term pyloric activity

Continuous, multi-day recordings of pyloric activity were analyzed in one of three ways: either as a list of burst times and their corresponding interburst intervals, as a spectrogram, or as an autocorrelogram. Activity metrics associated with each technique are listed in table 1. We define a "stable epoch" differently depending on the analysis method used, but in each case search for stable epochs began 15 hours following decentralization. For every long-term visualization of a decentralized preparation presented in this paper, time 0 corresponds to decentralization.

As a precursor to spectrogram and autocorrelogram analysis, *lvn* and *pdn* recordings were smooth rectified using an order 8 Chebyshev Type I low-pass filter with a 30 Hz cutoff frequency. Recordings were then downsampled from 2000 Hz to 80 Hz in order to make analysis more computationally manageable. Downsampled data lost information about fast spiking dynamics, but captured the slow (< 3 Hz) rhythm of the pyloric circuit that we were interested in. An example of a raw and downsampled *lvn* recording are shown in figure 2. Interburst interval analysis did not require smooth rectification or downsampling.

Table 1: Activity metrics. List of activity metrics, what they attempt to measure, and which analysis technique they are computed from.

Name	Measured feature of activity	Computed from
IBI	Speed	List of ISIs
σ_{ibis}	Variability	List of IBIs
Frequency*	Speed	Spectrogram
p_{peaks}/p_{total}*	Regularity	Spectrogram
p10	Activity level	Spectrogram
p3	Activity level	Spectrogram
p3/p10	Activity level	Spectrogram
lag_{peak1}*	Speed	Autocorrelogram
ACF_{peak1}*	Regularity	Autocorrelogram
P95median	Presence of dominant frequency or lag	Spectrogram and autocorrelogram

*Metric only computed for times when P95Median above threshold.

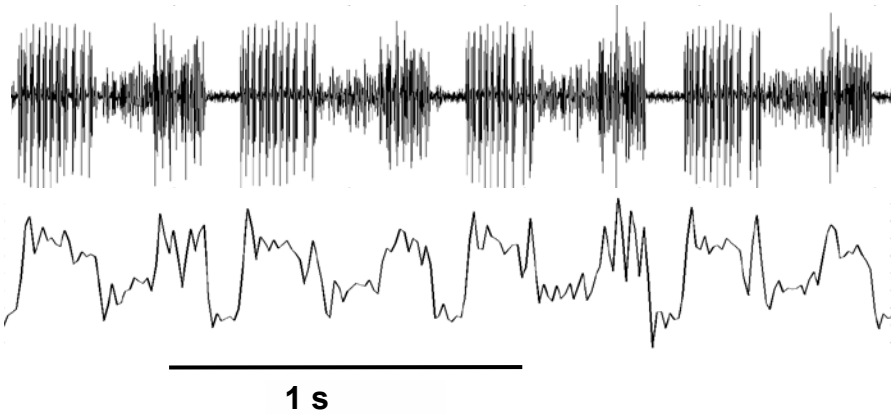

Figure 2: Recordings were downsampled before spectrogram and autocorrelogram analyses. Sample *lvn* recording before smooth rectification and downsampling (top) and after (bottom) from a control (no-treatment) preparation before decentralization.

Interburst interval analysis

Custom MATLAB scripts were used to extract spike times from extracellular recordings. Spike detection was performed on recordings from the *pdn* whenever available, otherwise on recordings from the *lvn*. Further analysis was done only on activity from the PD neurons, which we used as a readout of pyloric activity. From our lists of PD spike times for each preparation, we generated corresponding lists of interspike intervals (ISIs). To visualize how the distribution of ISIs change over time, we divided our lists of ISIs spanning multiple days into 30 minute bins. Within these 30 minute time bins, we further grouped ISIs of similar length using 0.01 second time bins. Histograms were created from these binned data with time bins represented along the x-axis, ISI-bins along the y-axis, and the number of ISIs falling in a given ISI bin within a given 30-minute time window represented by color. To focus on timing of PD bursts, we defined a cutoff ISI for each preparation above which ISIs corresponded to intervals between bursts. We refer to the ISIs falling above this cutoff as "interburst intervals" (IBIs). For decentralized preparations, a stable epoch was defined in terms of IBIs as a window of at least four hours during which the median filtered (order 5) IBIs stayed below 5 seconds.

The IBI analysis was used to analyze activity variability. To quantify how local variability changes over time, we used a rolling 2 hour window in which we computed the standard deviation of IBIs. We call this metric "σ_{IBIs}". Because of limitations in our spike detection algorithm, IBI analysis was performed only on a subset (n = 7) of our total decentralized sample: one chABC treated, one DNchABC treated, and 5 media-only preparations.

Spectrogram analysis

Spectrograms were created using MATLAB's spectrogram function with a 20 minute Hamming window and 50 percent overlap between successive segments. A spectrogram for a

given preparation was generated either entirely from the *lvn* recording, or entirely from the *pdn* recording. Each column of a spectrogram contains the power spectral density of frequency content during the temporal window corresponding to that column. As measures of overall activity level, we summed the total power up to 3 Hz and up to 10 Hz for each column of our spectrograms. We refer to these metrics as "p3" and "p10", respectively. To quantify the relative fraction of power that falls in the 0-3 Hz range, which would include typical pyloric rhythm frequencies, we also computed total power in the 0-3 Hz band divided by total power in the 0-10 Hz band. We call this metric "p3/p10". Additionally, for each spectrogram column we subtracted the median power from the 95th percentile of power. We call this metric "P95Median". A higher P95Median value indicates the presence of a dominant frequency, while a lower value indicates a flatter power spectrum. This metric more directly measures the presence of a dominant frequency as opposed to the overall power level across many frequencies measured by our activity-level metrics. We defined a P95Median threshold above which we considered a dominant frequency to be present (figure 3). The same threshold was used for all preparations. For times at which P95Median fell above this threshold, we further computed pyloric frequency and regularity. Pyloric frequency was found by first determining a subset of frequencies corresponding to the highest amplitude peaks in the power spectrum. Pyloric frequency was defined as the minimum frequency from this subset. To quantify regularity of the pyloric rhythm, we measured the fraction of total power that is accounted for by the previously computed pyloric frequency and its harmonics (figure 4). We call this metric "p_{peaks}/p_{total}". This metric's validity in quantifying regularity is illustrated by its appropriate quantification of activity regularity for two sine waves with equal mean period length, but different period length variability (figure 4 A&B). The power spectra for these sine waves contain a single peak, thus in our regularity metric the power under

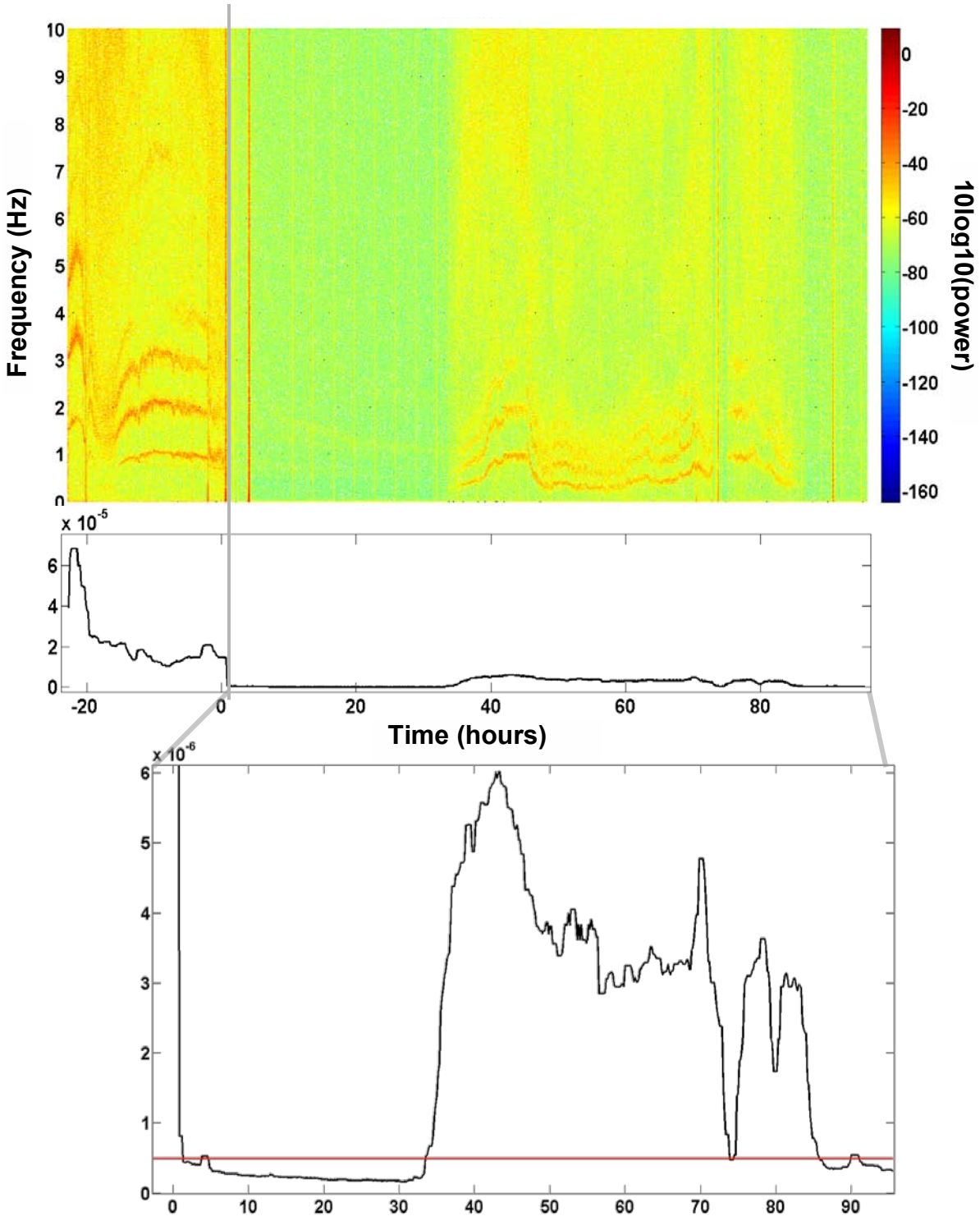

Figure 3: P95Median metric was used to define presence of dominant frequency. Spectrogram for a decentralized control (no-treatment) preparation (top) and corresponding trace of P95Median over time (middle). Bottom: P95Median trace highlighting hours 0-90. Threshold used to define presence of dominant frequency shown in red. Vertical grey line indicates decentralization.

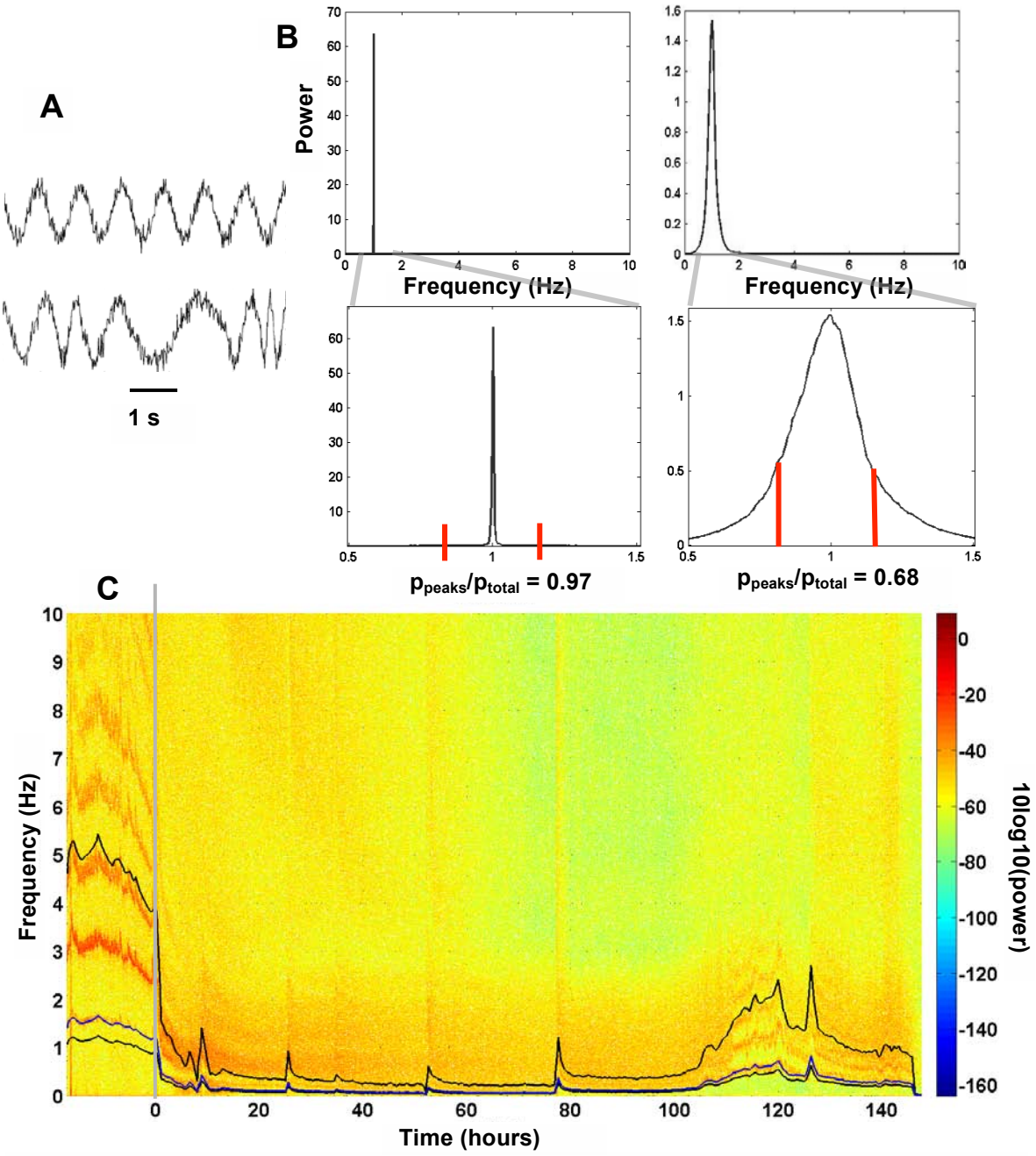

Figure 4: Quantifying pyloric rhythm regularity. (A) Sample artificial data used to illustrate validity of rhythm regularity metric. Sine waves were generated where each cycle period was drawn from a normal distribution. μ_{Period} = 1 s and σ_{Period} was varied. Top: σ_{Period} = 0.02 s. Bottom: σ_{Period} = 0.2 s. (B) Power spectra of sine waves with σ_{Period} = 0.02 s (left) and σ_{Period} = 0.2 s (right). Red lines indicate bandwidth over which to sum power for "p_{peaks}". "p_{total}" was summed from 0 to 10 Hz. Rhythm regularity, defined by p_{peaks}/p_{total}, is higher for the sine wave with lower period variability. (C) Spectrogram for a decentralized control (no treatment) preparation. Blue line traces pyloric frequency over time and black lines indicate bandwidth over which to sum for "p_{total}" quantity in p_{peaks}/p_{total} metric. This bandwidth scales according to changing pyloric frequency so that regularity measured by p_{peaks}/p_{total} is not confounded by changes in pyloric rhythm speed. Vertical grey line indicates decentralization.

this peak was divided by total power summed over the same bandwidth for each sine wave (0-10 Hz). This metric's application to pyloric rhythm is illustrated in figure 4C. Because the power spectra from our nerve recordings contain peaks at the pyloric rhythm frequency and its harmonics, we compensated for changes in frequency over time by scaling the "p_{total}" quantity in our metric according to the current pyloric frequency, thus ensuring that regularity as measured by p_{peaks}/p_{total} was not confounded by changes in activity speed. We defined a frequency range from pyloric frequency F – 0.25F to 3F + 0.25F. We then found the 3 frequencies (F_1, F_2, F_3) within this range with the highest amplitude peaks in the power spectrum. We summed the power from F_i-0.25F to F_i+0.25F for each of the 3 frequencies. F_1, F_2, and F_3 were chosen such that there was no overlap between each range F_i-0.25F to F_i+0.25F. The total power accounted for by F_1, F_2, and F_3 was divided by the total power from F – 0.25F to 3F + 0.25F, giving a value between 0 and 1 for p_{peaks}/p_{total} that quantifies the regularity of pyloric rhythm at the current time point. Our p3, p10, p3/p10, and P95Median metrics were smoothed using median filtering. Frequency and p_{peaks}/p_{total} were processed using LOWESS smoothing. For decentralized preparations, a stable epoch was defined in terms of our spectrogram analysis as a window of at least four hours during which a dominant frequency was present and stayed above 0.2 Hz.

Autocorrelogram analysis

The autocorrelation function (ACF) gives the similarity of observations as a function of the time lag between them. The ACF at lag *k* is the cross correlation of a signal with the same signal shifted temporally by lag *k*. Given a signal y with length L, mean $\bar{y}$, and sample variance c_0, the ACF at lag k is given by

$$ACF_k = \frac{c_k}{c_0}$$

where

$$c_k = \frac{1}{L}\sum_{t=1}^{L-k}(y_t - \bar{y})(y_{t+k} - \bar{y})$$

The ACF can range from -1, indicating perfect anticorrelation, to 1, indicating perfect correlation. Since a signal is always perfectly correlated with itself without any temporal lag, ACF_0 always equals 1. The ACF provides information about the periodicity of a signal. The ACF for a periodic signal with period *T* would have peaks when lag = T, lag = 2T, lag = 3T, etc. For a perfectly periodic signal, the amplitude of peaks in the ACF would remain constant with increasing lag. If a signal's period is variable, the amplitude of the first peak in the ACF will decrease to a value less than one and the amplitude of subsequent peaks will attenuate more rapidly.

To visualize changes in pyloric activity over time, we created autocorrelograms with time represented on the x-axis, temporal lag on the y-axis, and the ACF value represented by color. The ACF was computed every 4 minutes on the subsequent 20 minutes of data. For each column of our autocorrelograms, the ACF was computed up to a temporal lag of 3 minutes. An example autocorrelogram is shown in figure 5. An autocorrelogram for a given preparation was generated either entirely from the *lvn* recording, or entirely from the *pdn* recording. As with our spectrogram analysis, we used a P95Median metric to detect the presence of a dominant temporal lag. For each column of our autocorrelograms, we subtracted the median ACF value from the 95th percentile ACF value. We defined a threshold above which we considered there to be a dominant lag. For time points with P95Median falling above this threshold, we computed the first lag > 0 where there was a peak in the ACF, corresponding roughly to pyloric period. This metric, which we call "lag_{peak1}", was computed by finding the highest 8 peaks in the ACF

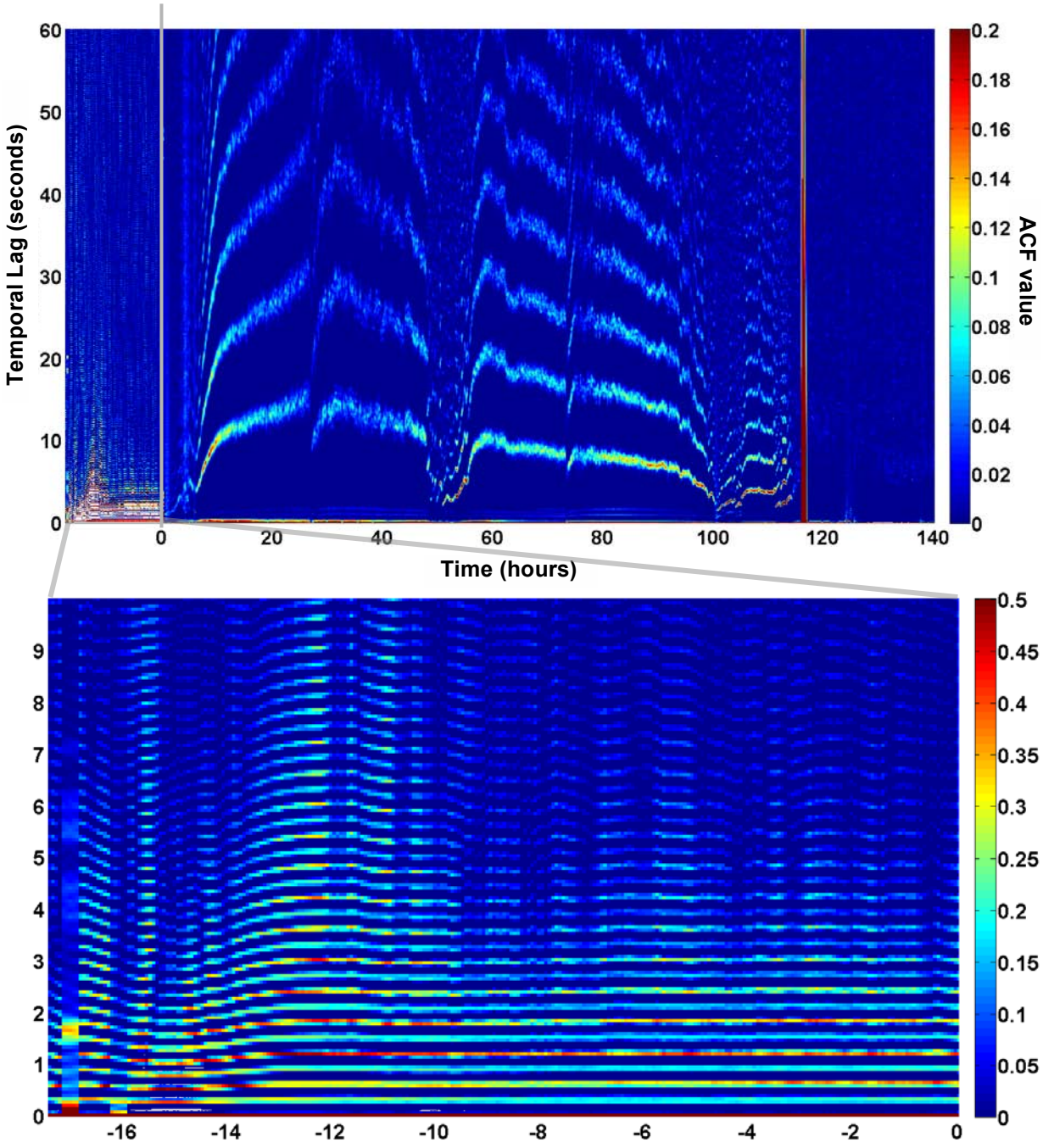

Figure 5: Example autocorrelogram. Autocorrelogram for a decentralized DNchABC-treated preparation. Vertical grey line indicates decentralization.

and their corresponding lags. We then selected the smallest lag from this subset. We quantified pyloric periodicity according the magnitude of the ACF at this selected lag. We call this value "ACF_{peak1}". Lag_{peak1} and ACF_{peak1} metrics were processed using LOWESS smoothing. For decentralized preparations, a stable epoch was defined in terms of our autocorrelogram analysis as a window of at least four hours during which a dominant lag was present and stayed below 5 seconds.

Statistical Analyses

Each of our metrics was computed over time for each preparation, quantifying how different aspects of pyloric activity vary over the hours following decentralization. Unstable epochs were defined as the time preceding distinct stable epochs. The first unstable epoch was defined to start 5 hours following decentralization. If two separate time ranges met our definition for stability and were separated by less than 4 hours, they were combined and analyzed as a single stable epoch. Thus each stable epoch was preceded by an unstable epoch of at least 4 hours. We refer to the onset time of the first stable epoch as "t_{stable}". We define preparations as having achieved stability if they enter at least one stable epoch following decentralization. The mean pre-decentralization value of a metric was defined as the mean value of that metric during the 10 hours preceding decentralization. In boxplots shown, outer edges of the box define the interquartile range (IQR). The red line in the middle of the box denotes the median. Whiskers extend to data points outside the IQR. Values more than 1.5(IQR) away from the 25^{th} or 75^{th} percentile are shown as individual points. All group means are reported as mean +/- standard error.

Among preparations that achieved stability regardless of treatment group, we computed the maximum average p_{peaks}/p_{total} and maximum average ACF_{peak1} that was attained during the 10

hours preceding decentralization, during unstable epochs, and during stable epochs. The maximum average was defined as the maximum value of a 4-hour moving average which scanned from beginning to end of an epoch. For preparations with two unstable or stable epochs, we computed the maximum average during both unstable epochs and both stable epochs and used the maximum from each epoch type. Maximum averages were only computed on windows where the P95Median was above its threshold for at least 25% of the window. Individuals without any qualifying 4-hour window during any unstable epoch were excluded from this analysis. Total sample size after excluding these individuals was 13 (no-treatment: n = 4; DNchABC: n = 5; chABC: n = 4). The maximum averages for each class of activity were compared using repeated measures ANOVA and Student's t-test with Bonferroni correction.

Among preparations that achieved stability, we compared t_{stable} between treatment groups (no-treatment: n = 5; DNchABC: n = 5; chABC: n = 4). For all preparations including those that did not achieve stability, we compared across treatment groups various measures of activity during hours 5-30 following decentralization. No preparation entered a stable epoch before hour 30. Individuals whose P95Median metric was above threshold for less than 25% of this time range were excluded from analyses that compared activity-dependent measures (frequency, p_{peaks}/p_{total}, lag_{peak1}, ACF_{peak1}). Total sample size after excluding these individuals was 16 for spectrogram-based activity-dependent measures (no-treatment: n = 4; DNchABC: n = 6; chABC: n = 6) and 13 for autocorrelogram-based measures (no-treatment: n = 3; DNchABC: n = 5; chABC: n = 5). All measures were normalized against their mean pre-decentralization values. Comparisons across treatment groups were made using one-way ANOVA and Tukey-Kramer tests.

Among preparations that achieved stability regardless of treatment group, we perform correlation analyses on measures summarizing activity during an unstable epoch with measures of activity during the subsequent stable epoch. Measures from the first unstable epoch are compared against measures from the first stable epoch. Measures from the first unstable epoch are also compared against t_{stable}. Among preparations that enter a second stable epoch, measures from the second unstable epoch are compared against measures from the second stable epoch. All measures were normalized against their mean pre-decentralization values. Individuals whose P95Median metric was above threshold for less than 25% of a given unstable epoch were excluded from analyses that compared activity-dependent measures (frequency, p_{peaks}/p_{total}, lag_{peak1}, ACF_{peak1}) between that epoch and the following stable epoch. Correlation was measured using Pearson's correlation coefficient, R.

RESULTS

IBI analysis inconclusive regarding activity variability and onset of stable epoch

Seven preparations were analyzed in terms of burst times and IBIs. One individual's activity following decentralization is displayed in terms of ISI length distribution over time in a histogram in figure 6B. This particular individual remained active following decentralization until onset of stable activity at hour 106. Local standard deviation of IBIs (σ_{IBIs}) is traced over time for the same individual in figure 6C. For this individual, σ_{IBIs} is maximized at hour 47. Hypothesizing that reaching maximal activity variability earlier might be conducive to achieving stability earlier, we next looked at the relationship between time of maximum σ_{IBIs} and t_{stable} across all seven individuals (figure 6D). No significant correlation was found between these two

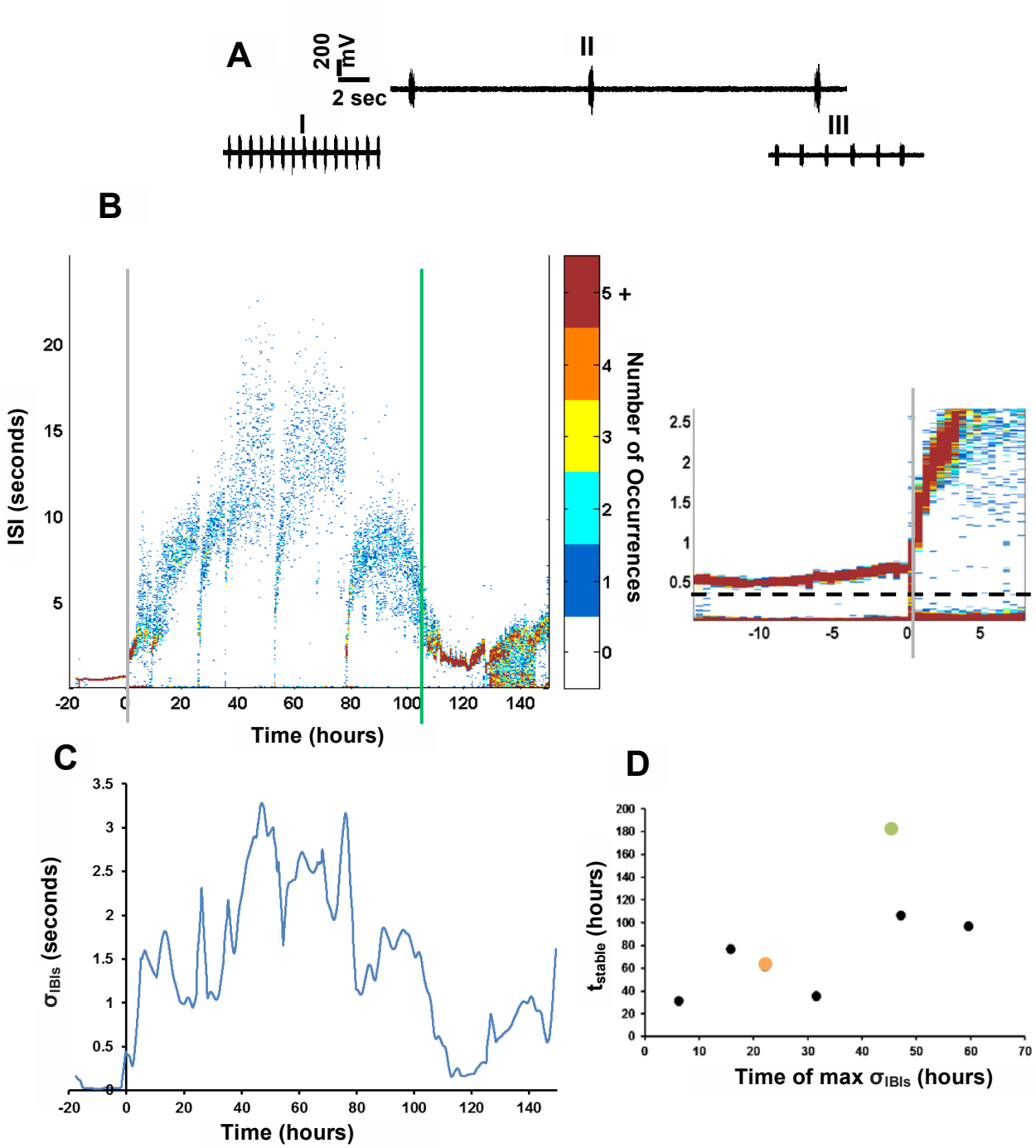

Figure 6: IBI analysis. (A) Sample from *pdn* recording before decentralization (I), 60 hours after decentralization (II), and during stable epoch (III). (B) Histogram of ISI lengths over time for individual control preparation (left) and expansion of same histogram illustrating cutoff ISI used to define IBIs (right). Vertical gray line indicates decentralization and vertical green line indicates t_{stable}. (C) Trace of standard deviation of IBIs over time for same individual shown in A. (D) t_{stable} versus time of max σ_{IBIs} ($R = 0.63$, $p = 0.13$). Black dots indicate no-treatment preparations. Orange dot indicates DNchABC-treated and green dot indicates chABC-treated.

measures ($p = 0.13$). We moved on to use spectrogram and autocorrelgoram analyses which allowed us to study a greater number of individuals.

Chondroitinase treated preparations show late onset of stability

In order to compare our definitions of stability with definitions of pyloric recovery used previously (Hudson 2013), we compared t_{stable} between treatment groups using both our frequency definition based on spectrogram analysis and our lag_{peak1} definition based on autocorrelogram analysis (figure 7A). Based on previous work, we expected to observe a delayed t_{stable} in the chABC group (Hudson 2013). According to our lag_{peak1}-based definition, one chABC treated individual entered a stable epoch (lasting ~4 hours) 28 hours following decentralization. Inspection of extracellular recording at this time revealed short bursts of fast pyloric activity lasting ~10 seconds followed by prolonged periods of silence lasting ~15 minutes. This stable epoch was not identified according to our frequency-based definition. Inspection of all other identified stable epochs for each preparation revealed consistent pyloric activity throughout the identified stable time range. The stable epoch identified at 28 hours was excluded and the next identified stable epoch (occurring at 134 hours) was used as t_{stable} for this individual. Among preparations that achieved stability, the mean t_{stable} in hours following decentralization was 65.3 +/- 14.9 (frequency definition) or 65.1 +/- 15.0 (lag_{peak1} definition) for no-treatment preparations, 68.6 +/- 6.8 (frequency definition) or 66.0 +/- 9.2 (lag_{peak1} definition) for DNchABC preparations, and 156.0 +/- 27.4 (frequency definition) or 140.0 +/- 20.4 (lag_{peak1} definition) for chABC preparations. One-way ANOVA revealed a significant difference in t_{stable} between the three treatment groups according to both the frequency-based definition ($p < 0.01$) and the lag_{peak1} definition ($p < 0.01$). Further, Tukey-Kramer tests revealed a significant delay in t_{stable} between the chABC group and both the no-treatment and DNchABC groups according to the frequency-

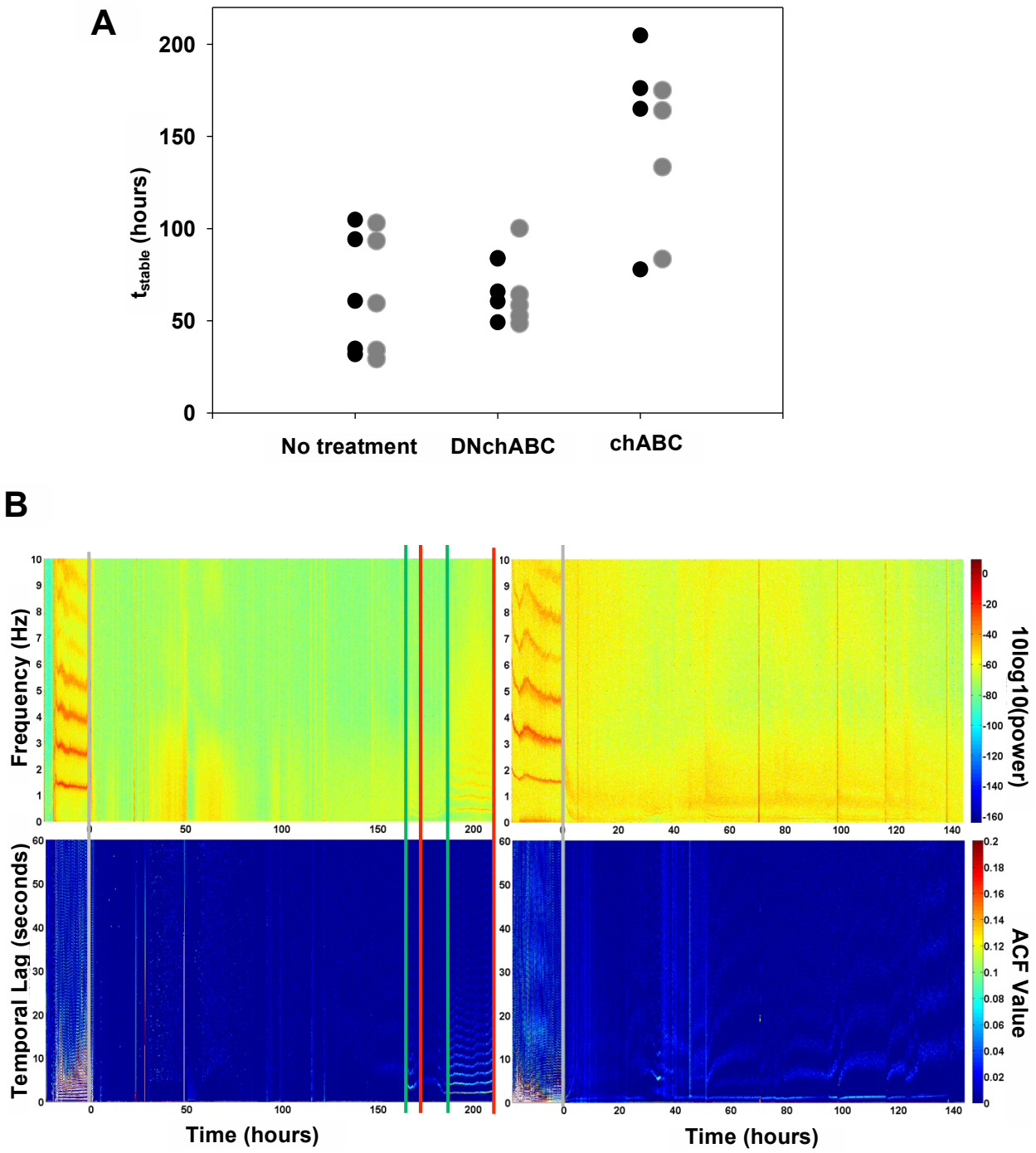

Figure 7: t_{stable} different across different treatment groups. (A) t_{stable} according to frequency-based definition (black) and lag_{peak1} definition (grey) across three different treatment groups. (B) chABC-treated individual that achieved stability (left) and chABC-treated individual that did not achieve stability (right). Vertical grey lines indicate decentralization, green lines indicate start of stable epoch, red lines indicate end of stable epoch.

based definition of stability (no-treatment: $p < 0.01$, DNchABC: $p < 0.05$). The lag_{peak1} definition of stability also revealed a significant delay in t_{stable} among chABC preparations compared to controls (no-treatment: $p < 0.05$, DNchABC: $p < 0.05$). No significant difference in t_{stable} was observed between no-treatment and DNchABC groups according to either definition (frequency-based: $p = 0.99$, lag_{peak1}-based: $p = 0.99$). These results are based on the same data used in the Hudson 2013 study, which previously reported chABC to delay t_{stable}, and are included here only to illustrate the effectiveness of our two definitions of stability. Among all preparations included in the present study, 5/5 no-treatment individuals, 5/6 DNchABC individuals, and 4/8 chABC individuals achieved stability. These results are consistent across both definitions of stability. Examples of chABC treated preparations that did and did not achieve stability are shown in figure 7B.

Activity regularity decreases following decentralization, but increases significantly during stable epochs

In our IBI analysis, we quantified activity variability. In our spectrogram and autocorrelogram analyses, we quantify activity regularity. Because in our IBI analysis we looked for a potential relationship between time of maximum activity variability and t_{stable}, it would be logical to analyze the relationship between time of minimum activity regularity and t_{stable}. However, after observing traces of p_{peaks}/p_{total} and ACF_{peak1} over time, no common temporal pattern in these two measures of regularity was observed across individuals. Multiple similar-magnitude minima in activity regularity would often be observed separated by hours of time, thus making identification of a single time of minimal activity regularity arbitrary and not meaningful. Example traces of p_{peaks}/p_{total} and ACF_{peak1} are shown for a DNchABC-treated individual in figure 8A and 8B.

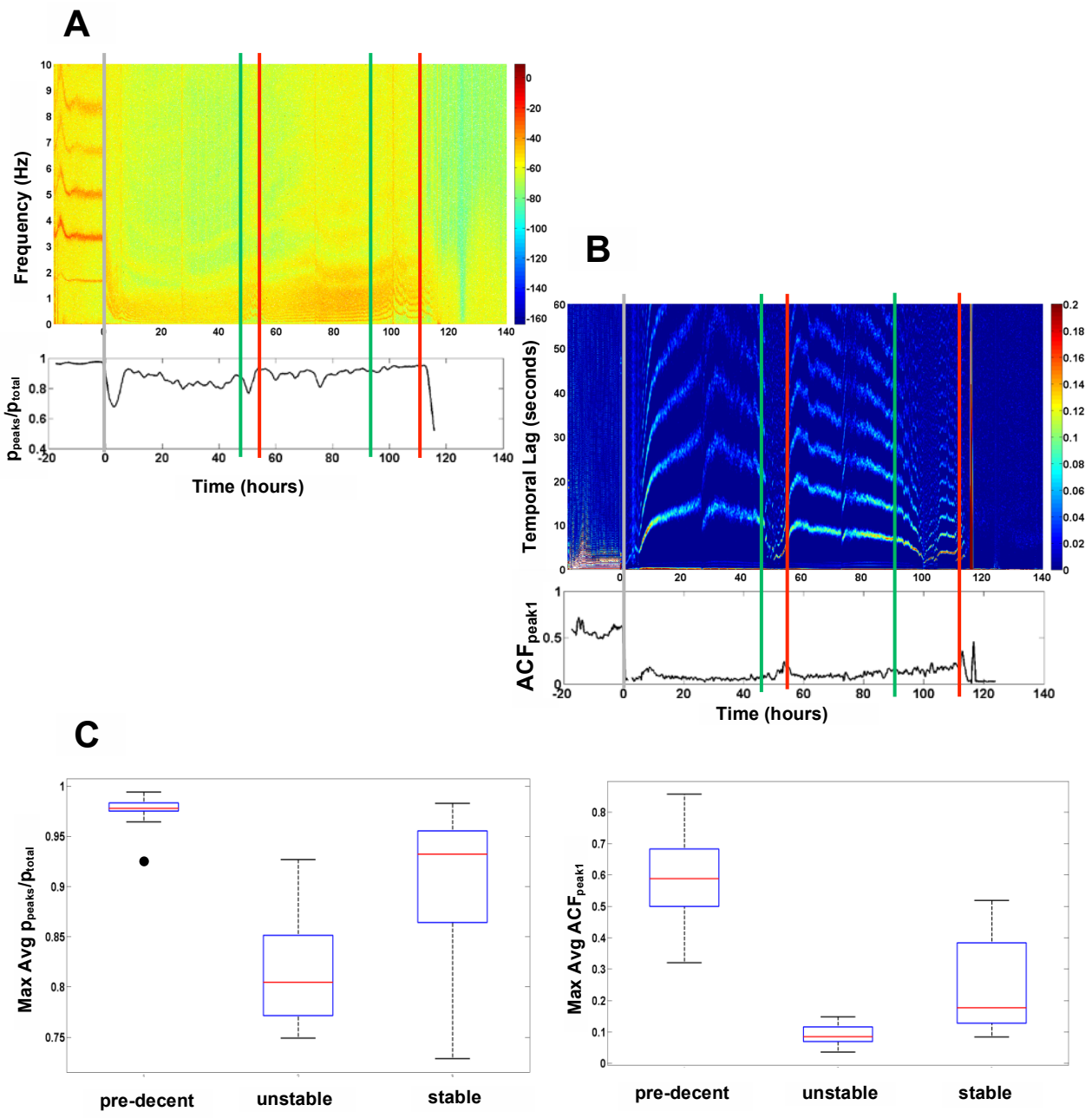

Figure 8: Pyloric rhythm regularity differs before decentralization and between stable and unstable epochs. (A) Spectrogram for DNchABC-treated preparation with corresponding trace of p_{peaks}/p_{total} over time. Color scale represents 10log10(power). (B) Autocorrelogram for same individual as in A with corresponding trace of ACF_{peak1} over time. Color scale represents ACF value. Vertical grey lines indicate decentralization, green lines indicate start of stable epoch, red lines indicate end of stable epoch. (C) Max average p_{peaks}/p_{total} (left) and max average ACF_{peak1} (right) across three different classes of pyloric activity. Includes individuals that achieved stability, regardless of treatment group (n = 13).

To quantify how activity regularity relates to class of pyloric activity, we compared the maximum average activity regularity before decentralization, during unstable epochs, and during stable epochs (figure 8C). Among individuals that achieved stability regardless of treatment group, repeated measures ANOVA revealed a significant difference between maximum average regularity during these three types of pyloric activity (p_{peaks}/p_{total}: < 0.001, ACF_{peak1}: $p < 0.001$). Pairwise comparisons using Bonferroni t-test revealed pre-decentralization max avg p_{peaks}/p_{total} (0.975 +/- 0.005) to be significantly higher than unstable max avg p_{peaks}/p_{total} (0.819 +/- 0.016, $p < 0.001$) and stable max avg p_{peaks}/p_{total} (0.906 +/- 0.023, $p < 0.01$). Unstable max avg p_{peaks}/p_{total} was also significantly lower than stable max avg p_{peaks}/p_{total} ($p < 0.001$). Similarly, pre-decentralization max avg ACF_{peak1} (0.590 +/- 0.041) was significantly higher than unstable max avg ACF_{peak1} (0.091 +/- 0.032, $p < 0.001$) and stable max avg ACF_{peak1} (0.249 +/- 0.042, $p < 0.001$). Unstable max avg ACF_{peak1} was also significantly lower than stable max avg ACF_{peak1} ($p < 0.01$). The same trends in mean maximum average regularity (pre-decentralization max avg regularity > stable max avg regularity > unstable max avg regularity) were seen within treatment groups (no-treatment: n = 4; DNchABC: n = 5; chABC: n = 4) for both p_{peaks}/p_{total} and ACF_{peak1}, however these differences were not consistently significant for either p_{peaks}/p_{total} or ACF_{peak1}. Long term visualizations of two intact (not decentralized) individuals and corresponding traces of p_{peaks}/p_{total} and ACF_{peak1} over time are shown in figure 9. For both individuals, speed of pyloric rhythm and activity regularity decrease over time, possibly explaining the decreased max average p_{peaks}/p_{totasl} and ACF_{peak1} observed in stable epochs compared to pre-decentralization values. It has been speculated that the gradual slowing of the pyloric rhythm *in vitro* may represent a shift toward a rhythm speed typical of a live, unfed animal. The rhythm speed

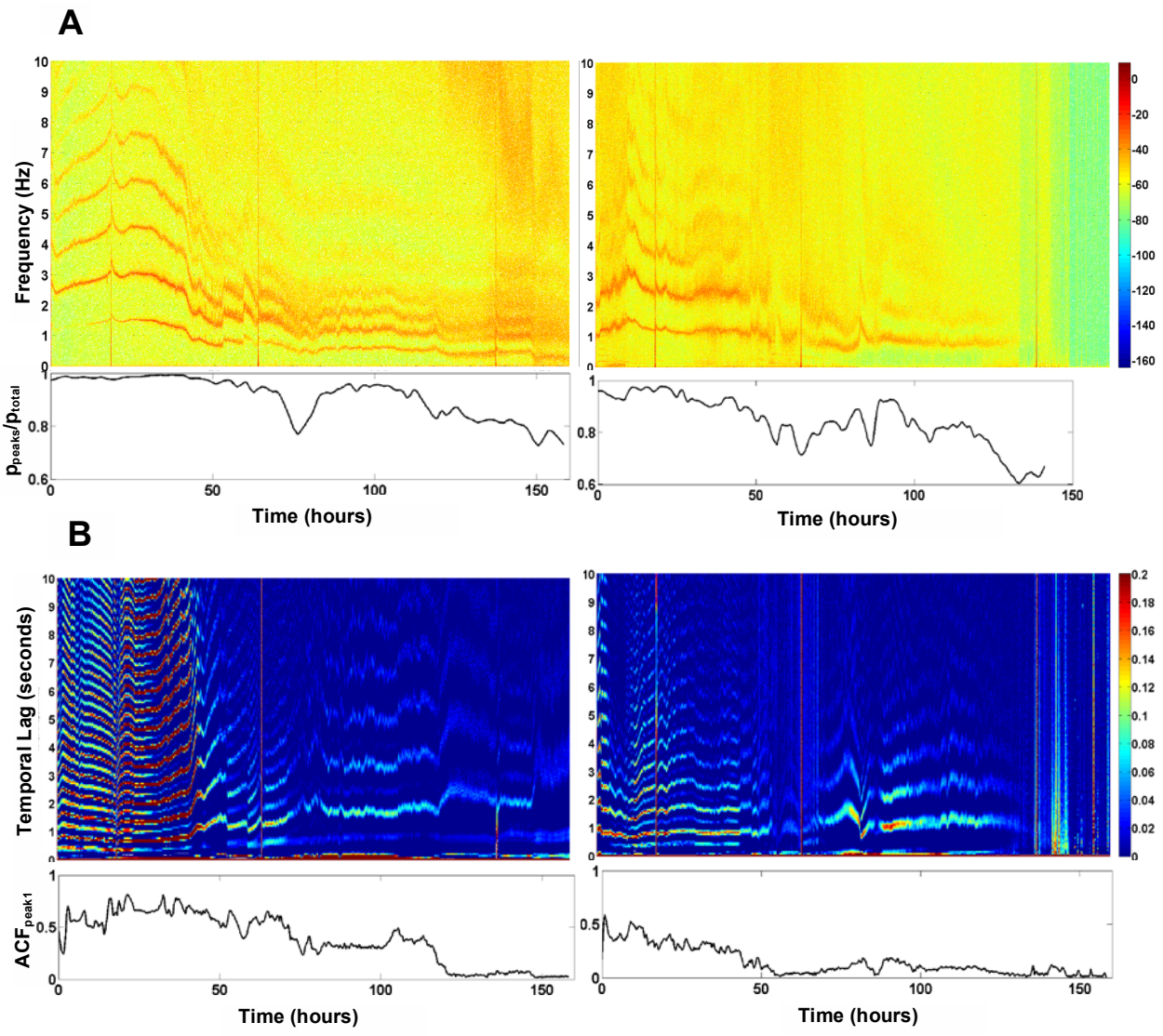

Figure 9: Long-term pyloric activity in two intact preparations. (A) Spectrograms of two untreated, intact preparations (top) and corresponding trace of p_{peaks}/p_{total} over time (bottom). Color scale represents 10log10(power). (B) Autocorrelograms for same two preparations as in A (top) and corresponding trace of ACF_{peak1} over time (bottom). Color scale represents ACF value.

observed immediately following excision of the STNS may be unusually fast due to removal of potentially suppressive inputs from the brain and sensory systems (Golowasch et al., 2009).

No significant differences found in activity following decentralization between treatment groups

In order to identify features of activity following decentralization that are predictive of an individual's ability to achieve stability, we compared various summary measures of activity during hours 5-30 following decentralization between treatment groups. ChABC is known to either delay or prevent the pyloric circuit from regaining stable rhythm following decentralization (Hudson 2013), so features of activity unique to chABC-treated preparations could provide information about how stability is achieved. We normalized all measures of activity by their mean pre-decentralization values in order to focus on how an individual's post-decentralization activity changes relative to its activity when the *stn* was intact. For example, "mean frequency" refers to the mean frequency during hours 5-30 normalized by the mean frequency in the 10 hours preceding decentralization for that individual. "Min frequency" refers to the minimum frequency during hours 5-30 normalized by the mean frequency in the 10 hours preceding decentralization. A complete list of compared measures is listed in table 2. One-way ANOVA did not reveal any significant differences between treatment groups for any measure tested (all p-values >= 0.18).

Testing for correlation between activity features in stable epoch and preceding unstable epoch

In addition to comparing post-decentralization activity features between treatment groups, we analyzed relationships between activity during a stable epoch and the preceding unstable epoch, looking for features of unstable activity that are predictive of features of stable

Table 2: Comparison of activity measures during hours 5-30 between treatment groups. All measures were normalized by their mean pre-decentralization value.

Normalized measure	**p-value (One-way ANOVA)**
Mean frequency*	0.65
Min frequency*	0.18
Mean p_{peaks}/p_{total}*	0.76
Min p_{peaks}/p_{total}*	0.92
Max p_{peaks}/p_{total}*	0.90
Mean p10	0.55
Mean p3	0.75
Mean p3/p10	0.80
Mean ACF_{peak1}*	0.68
Min ACF_{peak1}*	0.61
Max ACF_{peak1}*	0.67
Mean lag_{peak1}*	0.28
Max lag_{peak1}*	0.25

***** Comparisons involving P95Median-dependent metrics exclude individuals whose P95Median metric was above threshold for less than 25% of the hour 5 – hour 30 time range (excludes 3 individuals for frequency and p_{peaks}/p_{total} measures, 6 individuals for lag_{peak1} and ACF_{peak1} measures).

activity. All measures were normalized by their mean pre-decentralization value. Only measures derived from the same type of analysis (either spectrogram or autocorrelogram) were compared. Among preparations that achieved stability regardless of treatment group, we compared activity measures from the first unstable epoch to measures from the first stable epoch. We additionally tested for correlation between activity during the first unstable epoch and t_{stable}. A complete list of all comparisons and their corresponding p-value for correlation tested using the Pearson correlation coefficient is shown in table 3. No significant correlations were found.

Across individuals, the first stable epoch had an average duration of 20 hours with a standard deviation of 25 hours (frequency-based stability definition) or an average duration of 21 hours with a standard deviation of 24 hours (lag_{peak1}-based stability definition). For each definition of stability, 6/14 individuals had two stable epochs. Among these individuals, the second stable epoch had an average duration of 27 hours with a standard deviation of 23 hours (frequency-based stability definition) or an average duration of 19 hours with a standard deviation of 10 hours (lag_{peak1}-based stability definition). We further tested for correlation between activity during the second unstable epoch and second stable epoch among these six individuals. Several measures were significantly correlated at the $\alpha = 0.05$ level of significance (figure 10). Figure 10A&B indicates a relationship between activity level during the unstable epoch and minimum activity regularity in the following stable epoch. However, these correlations appear highly dependent on a single data point. Due to the small sample size ($n = 6$), the robustness of this correlation is unclear. Figure 10 D&E indicate a correlation between maximum activity regularity during the unstable epoch and maximum or mean activity regularity during the stable epoch. These correlations seem especially strong, however for 3/5 individuals, the unstable max ACF_{peak1} occurred within 1 hour of either the end of the previous stable epoch

Table 3: Correlation tests between activity measures during 1st unstable epoch and 1st stable epoch. All measures were normalized by their mean pre-decentralization value. Entries in table indicate p-values for Pearson correlation test between indicated measures.

1st Unstable Epoch	1st Stable Epoch: Mean freq*	Max freq*	Mean p_{peaks}/p_{total}*	Min p_{peaks}/p_{total}*	Max p_{peaks}/p_{total}*	Mean lag_{peak1}*	Min lag_{peak1}*	Mean ACF_{peak1}*	Min ACF_{peak1}*	Max ACF_{peak1}*	t_{stable}
Mean freq*	0.92	0.36	0.96	0.76	0.58						0.62
Min freq*	0.56	0.69	0.55	0.23	0.39						0.23
Mean p_{peaks}/p_{total}*	0.72	0.69	0.53	0.21	0.29						0.09
Min p_{peaks}/p_{total}*	0.60	0.95	0.28	0.12	0.15						0.41
Max p_{peaks}/p_{total}*	0.79	0.22	0.25	0.40	0.05 (0.053)						0.80
Mean p10	0.60	0.98	0.30	0.84	0.80						0.65
Mean p3	0.18	0.29	0.86	0.21	0.97						0.46
Mean p3/p10	0.18	0.22	0.99	0.22	0.98						0.54
Mean lag_{peak1}*						0.65	0.58	0.19	0.80	0.61	0.42
Max lag_{peak1}*						0.81	0.88	0.93	0.88	0.88	0.09
Mean ACF_{peak1}*						0.47	0.55	0.96	0.29	0.90	0.62
Min ACF_{peak1}*						0.25	0.36	0.74	0.73	0.91	0.77
Max ACF_{peak1}*						0.81	0.90	0.53	0.49	0.47	0.98

***** Correlations involving P95Median-dependent metrics exclude individuals whose P95Median metric was above threshold for less than 25% of any epoch (excludes 1 individual for frequency and p_{peaks}/p_{total} measures, 3 individuals for lag_{peak1} and ACF_{peak1} measures).

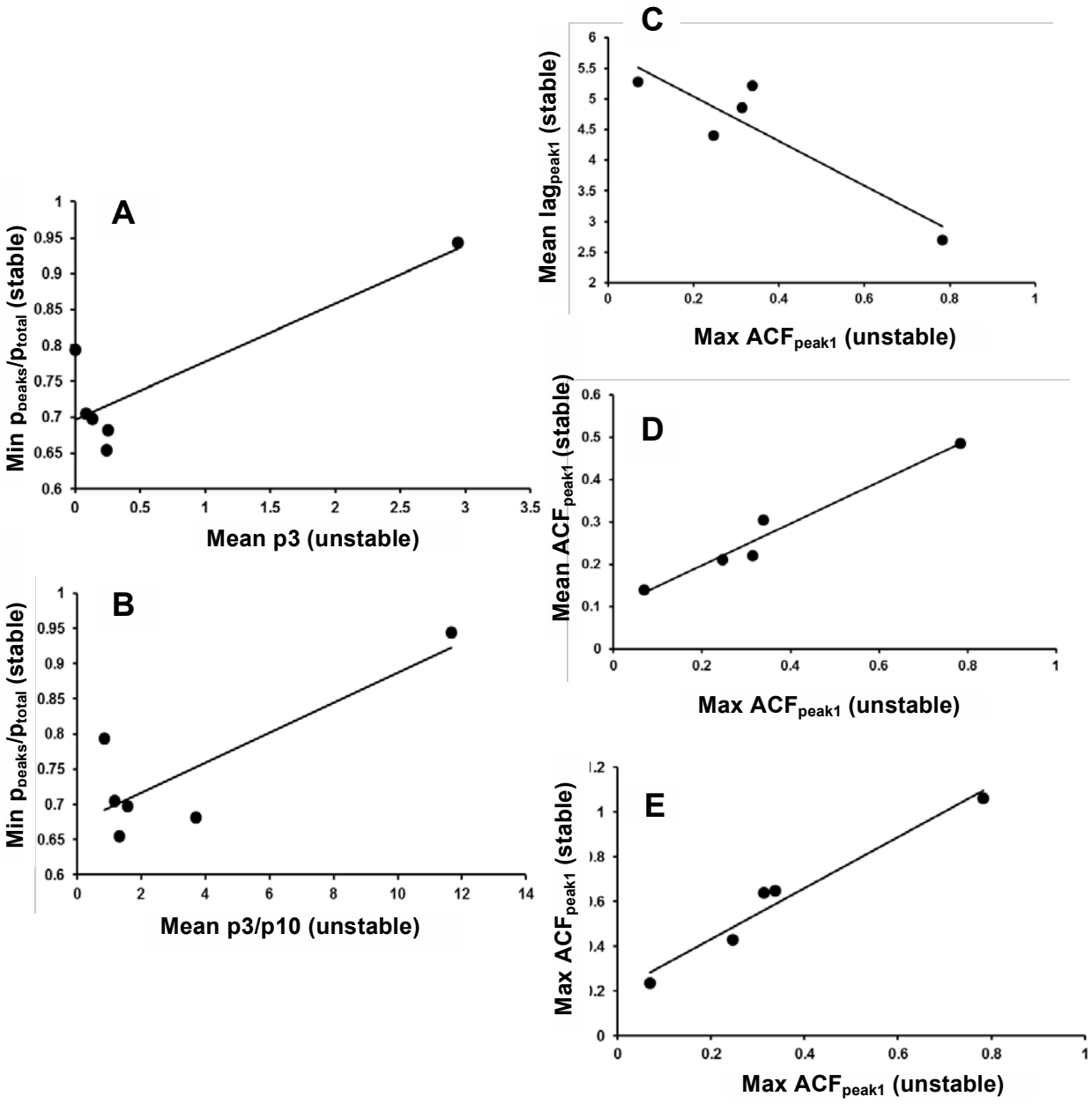

Figure 10: Correlations between activity measures during 2nd unstable epoch and 2nd stable epoch. All measures were normalized by their mean pre-decentralization value. (A) R = 0.86, p = 0.03. (B) R = 0.83, p = 0.04. (C) R = -0.90, p = 0.04. (D) R = 0.96, p = 0.003. (E) R = 0.98, p = 0.004.

or start of the subsequent stable epoch, suggesting that these correlations may in reality indicate a relationship in activity regularity between two stable epochs in the same individual, which is not surprising. Figure 10C indicates that as maximum activity regularity increases during the unstable epoch, the mean lag_{peak1} in the subsequent stable epoch decreases. Regardless of when the unstable max ACF_{peak1} occurred, this could indicate higher previous activity regularity correlates with slower eventual stable rhythm. When considering the correlations presented in figure 10, it is important to note that we tested for more than 60 potential correlations. While a Bonferroni correction for this large number of tests would be too conservative, a Bonferroni correction for only 3 comparisons would set $\alpha = 0.017$, at which level the correlations presented in figure 10A, 10B, and 10C would not be considered significant.

We did not test for correlations within treatment groups. For activity-dependent measures such as pyloric frequency or lag_{peak1} in which we excluded individuals whose P95Median value was not above threshold for at least 25% of a given epoch, our sample size dropped to n = 3 for controls and n = 3 for chABC-treated preparations. A correlation analysis on such a low sample size would not give convincing evidence for or against a relationship between two activity measures.

DISCUSSION

The objective of this study was two-fold. First, we aimed to study the pyloric circuit's ability to functionally recover after being isolated from neuromodulatory input. In particular, we aimed to conduct an in-depth study of the pyloric circuit's electrical activity in response to decentralization. The reemergence of stable pyloric rhythm following decentralization takes

several days. We were particularly interested in the unstable activity that follows decentralization and whether or how it relates to stable activity that may or may not be achieved later. Because degradation of extracellular matrix via chABC treatment is known to delay or prevent reemergence of stable activity, we also looked for potential differences in activity across treatment groups during the 30 hours following decentralization. Our goal of studying pyloric activity in detail across multiple days motivated our second aim: to develop multiple ways of visualizing long-term neuronal activity and to quantify how different features of activity change over time.

Three ways of analyzing pyloric activity

We analyzed long-term pyloric activity in three ways: as burst times and interburst intervals, which we visualized in a histogram, as a spectrogram, and as an autocorrelogram. For each technique, we developed a set of metrics that can be used to describe different aspects of neuronal activity. Several different metrics described the same or related features of activity. For example, we used both p_{peaks}/p_{total} and ACF_{peak1} to describe activity regularity and σ_{IBIs} to describe activity variability. In general, variability and regularity are measures that can be defined in many ways. Finding multiple definitions to apply to neuronal activity has thus strengthened our analysis.

Our IBI analysis was based on spike detection, one of the most common ways in neuroscience to study neuronal activity. Accurate spike detection can allow for a detailed analysis of activity on small timescales and can often distinguish between different neuron types. When working with long-term extracellular recordings, however, accurate spike detection becomes challenging. Spectrograms and autocorrelograms can be generated from raw waveforms without any intermediate spike detection step. This allows for easy visualization of long-term

processes without first having to optimize a spike detection algorithm. However, error is introduced when extracting features such as frequency from a spectrogram or first nonzero peak from an autocorrelogram. Additionally, our spectrograms and autocorrelograms were generated on relatively course timescales and thus do not give a good representation of fast changes in neuronal activity. For example, pyloric bouting can occur in which several short spurts of fast activity are separated by longer periods of slow activity or silence. If these dramatic shifts in activity speed occurred within the temporal window of a spectrogram or autocorrelogram, the timing of shifts between these two distinct activity types could not be detected. Our spectrograms and autocorrelograms, which use temporal windows on the order of minutes, are thus better equipped to detect more gradual changes in activity. Each of our three analysis techniques has its strengths and weaknesses. Spectrograms and autocorrelograms are particularly powerful tools to provide a big-picture description of long-term electrical activity.

Activity regularity decreases following decentralization and increases upon reemergence of stable activity

Because our definitions of stability required only a sufficiently fast rhythm with no minimum requirement for activity regularity, we quantified maximum average activity regularity during three types of pyloric activity: pre-decentralization, unstable, and stable. Among all individuals that achieved stability, we found that activity regularity is significantly higher during stable epochs as compared to unstable epochs, but significantly lower than before decentralization. This result was consistent across both definitions of regularity. However, these differences in maximum average activity regularity were not consistently significant within treatment groups for either definition of regularity. This lack of observable difference may be due to small within-treatment group size. Further data would need to be collected to draw a

strong conclusion. Nevertheless, that maximum average regularity increases significantly during time ranges we define as stable would not be surprising biologically. For our stable epochs to truly represent a functional recovery, the pyloric circuit would need to regain the regularity that was lost following decentralization. As a central pattern generator, the pyloric circuit must maintain a highly periodic rhythm in order to serve its biological function.

Lack of evidence for post-decentralizaton activity features that are predictive of stable activity

In an effort to better understand the pyloric circuit's ability to adapt following decentralization, we attempted to identify any feature of activity following decentralization that either differed significantly between treatment groups or was predictive of some quality of stability achieved later. Because chABC treatment is known to affect the pyloric circuit's ability to functionally recover following decentralization without affecting ongoing activity when the *stn* is left intact (Hudson 2013), we first looked for features of activity that differed significantly across treatment groups in the 30 hours following decentralization. No measure we tested was found to be significantly different between groups, suggesting that the underlying mechanism responsible for chABC's effect is not evident from electrical activity alone. We only tested for differences in activity during hours 5-30 following decentralization in order to compare over time ranges of equal length in which no individual had entered a stable epoch. However, gene transcription in the hours immediately following decentralization has been shown to be critical for eventual rhythm recovery. Functional recovery can be prevented by application of an RNA-synthesis inhibitor at the time of decentralization (Thoby-Brisson and Simmers 2000). Given this evidence for the importance of the time following decentralization at a gene-transcription level, it

is interesting that no differences in electrical activity between treatment groups were observed during a similar time window.

Among individuals that achieved stability regardless of treatment group, we additionally tested for correlation in activity patterns between an unstable epoch and the following stable epoch. Our analysis on the relationship between activity during unstable epoch one and stable epoch one revealed no significant correlations. The same analysis conducted on unstable epoch two and stable epoch two (among individuals that entered two stable epochs) revealed several correlations that were significant at the $\alpha = 0.05$ level of significance. Further analysis of the strongest two correlations indicate that they represent a relationship between activity during the first and second stable epoch rather than between activity during unstable epoch two and stable epoch two. The remaining correlations identified would not be considered significant with an α-level adjusted for as few as three comparisons using the Bonferroni correction.

How to look for activity qualities that are predictive of activity during a second stable epoch was not immediately clear. We chose to test for potential correlations between unstable epoch two and stable epoch two as a distinct group since activity measures for these epochs are not independent of measures describing earlier epochs. However, our analysis could have missed potentially predictive features of activity preceding unstable epoch two. Given that the vast majority of correlations tested were not significant at even the $\alpha = 0.05$ level of significance, we do not find strong evidence that features of activity during stability can be predicted by features of activity during preceding unstable activity.

Significance and future directions

Our results altogether do not indicate electrical activity following decentralization to be a clear indicator of whether stability is eventually achieved or the regularity or speed of

reemerging stable pyloric rhythm. These results may seem surprising given that electrical activity is a known feedback mechanism for regulating membrane properties such as cellular conductance (Le Masson et al., 1993; Turrigiano et al.,1994; Liu et al., 1998; Golowasch et al. 1999). Evidence that neuromodulator-dependent mechanisms also regulate ion channel densities and play a key role in the recovery process (Zhang et al., 2009; Zhang and Golowasch 2011; Khorkova and Golowasch 2007; Temporal et al., 2012) may explain why electrical activity alone cannot predict features of the circuit's adaptive ability. Bouting behavior has previously been found not to be predictive of recovery (Luther et al., 2003). It has been speculated that variability in bouting behavior may be explained by differential states of cellular conductances before decentralization (Luther et al., 2003). Our results thus extend further to suggest that more gradual-long term electrical activity dynamics are also not predictive of later activity stability. Experimental evidence suggests that post-decentralization activity patterns and onset of time of stable activity can be altered by manipulating the activity and neuromodulator environment of the pyloric circuit prior to decentralization (Zhang et al., 2009). Thus while the present study focused on differential post-decentralization activity across individuals, it would be interesting in the future to assess the relationship between pre-decentralization activity and post-decentralization stability. Our results suggest that analysis of post-decentralization activity alone may not provide information about the ability of the pyloric circuit to achieve stability following decentralization.

REFERENCES

Bal, T., Nagy, F., & Moulins, M. (1988). The pyloric central pattern generator in crustacea: a set of conditional neuronal oscillators. *Journal of Comparative Physiology A*, *163*(6), 715-727.

Foster, W. R., Ungar, L. H., & Schwaber, J. S. (1993). Significance of conductances in Hodgkin-Huxley models. *Journal of neurophysiology*, *70*(6), 2502-2518.

Goldman, M. S., Golowasch, J., Marder, E., & Abbott, L. F. (2001). Global structure, robustness, and modulation of neuronal models. *The Journal of Neuroscience*, *21*(14), 5229-5238.

Golowasch, J., Casey, M., Abbott, L. F., & Marder, E. (1999). Network stability from activity-dependent regulation of neuronal conductances. *Neural computation*, *11*(5), 1079-1096.

Golowasch, J., Goldman, M. S., Abbott, L. F., & Marder, E. (2002). Failure of averaging in the construction of a conductance-based neuron model. *Journal of Neurophysiology*, *87*(2), 1129-1131.

Harris-Warrick, R. M. (Ed.). (1992). *Dynamic biological networks: the stomatogastric nervous system* (28-29; 89-91). MIT Press.

Hudson, A. E. (2013). *Neuronal mechanisms for the maintenance of consistent behavior in the stomatogastric ganglion of Cancer borealis* (Doctoral dissertation). Retrieved from http://hdl.handle.net/1853/47654

Hudson, A. E., Archila, S., & Prinz, A. A. (2010). Identifiable cells in the crustacean stomatogastric ganglion. *Physiology*, *25*(5), 311-318.

Khorkova, O., & Golowasch, J. (2007). Neuromodulators, not activity, control coordinated expression of ionic currents. *The Journal of neuroscience*, *27*(32), 8709-8718.

LeMasson, G., Marder, E., & Abbott, L. F. (1993). Activity-dependent regulation of conductances in model neurons. *Science*, *259*, 1915-1915.

Liu, Z., Golowasch, J., Marder, E., & Abbott, L. F. (1998). A model neuron with activity-dependent conductances regulated by multiple calcium sensors. *The Journal of neuroscience*, *18*(7), 2309-2320.

Luther, J. A., Robie, A. A., Yarotsky, J., Reina, C., Marder, E., & Golowasch, J. (2003). Episodic bouts of activity accompany recovery of rhythmic output by a neuromodulator- and activity-deprived adult neural network. *Journal of neurophysiology*, *90*(4), 2720.

Moulins, M., & Cournil, I. (1982). All-or-none control of the bursting properties of the pacemaker neurons of the labster pyloric pattern generator. *Journal of neurobiology*, *13*(5), 447-458.

Marder, E., & Bucher, D. (2007). Understanding circuit dynamics using the stomatogastric nervous system of lobsters and crabs. *Annual Review of Physiology*, *69*, 291-316.

Prinz, A. A., Billimoria, C. P., & Marder, E. (2003). Alternative to hand-tuning conductance-based models: construction and analysis of databases of model neurons. *Journal of Neurophysiology*, *90*(6), 3998-4015.

Prinz, A. A., Bucher, D., & Marder, E. (2004). Similar network activity from disparate circuit parameters. *Nature neuroscience*, *7*(12), 1345-1352.

Rezer, E., & Moulins, M. (1983). Expression of the crustacean pyloric pattern generator in the intact animal. *Journal of comparative physiology*, *153*(1), 17-28.

Schulz, D. J., Goaillard, J. M., & Marder, E. (2006). Variable channel expression in identified single and electrically coupled neurons in different animals. *Nature neuroscience*, *9*(3), 356-362.

Selverston, A. I., Russell, D. F., Miller, J. P., & King, D. G. (1976). The stomatogastric nervous system: structure and function of a small neural network. *Progress in neurobiology*, *7*, 215-289.

Thoby-Brisson, M., & Simmers, J. (2002). Long-term neuromodulatory regulation of a motor pattern–generating network: maintenance of synaptic efficacy and oscillatory properties. *Journal of neurophysiology*, *88*(6), 2942-2953.

Thoby-Brisson, M., & Simmers, J. (2000). Transition to endogenous bursting after long-term decentralization requires de novo transcription in a critical time window. *Journal of neurophysiology*, *84*(1), 596-599.

Thoby-Brisson, M., & Simmers, J. (1998). Neuromodulatory inputs maintain expression of a lobster motor pattern-generating network in a modulation-dependent state: evidence from long-term decentralization in vitro. *The Journal of neuroscience*, *18*(6), 2212-2225.

Temporal, S., Desai, M., Khorkova, O., Varghese, G., Dai, A., Schulz, D. J., & Golowasch, J. (2012). Neuromodulation independently determines correlated channel expression and conductance levels in motor neurons of the stomatogastric ganglion. *Journal of neurophysiology*, *107*(2), 718-727.

Turrigiano, G., Abbott, L. F., & Marder, E. (1994). Activity-dependent changes in the intrinsic properties of cultured neurons. *Science*, *264*(5161), 974-976.

Zhang, Y., & Golowasch, J. (2011). Recovery of rhythmic activity in a central pattern generator: analysis of the role of neuromodulator and activity-dependent mechanisms. *Journal of computational neuroscience*, *31*(3), 685-699.

Zhang, Y., & Golowasch, J. (2007). Modeling recovery of rhythmic activity: hypothesis for the role of a calcium pump. *Neurocomputing*, *70*(10), 1657-1662.

Zhang, Y., Khorkova, O., Rodriguez, R., & Golowaschi, J. (2009). Activity and Neuromodulatory Input Contribute to the Recovery of Rhythmic Output After Decentralization in a Central Pattern Generator. *Journal of neurophysiology*, *101*, 372-386.